International Journal of Solids and Structures 45 (2008) 5397–5418

Contents lists available at ScienceDirect

International Journal of Solids and Structures

journal homepage: www.elsevier.com/locate/ijsolstr

Strain gradient plasticity analysis of transformation induced plasticity in multiphase steels

L. Mazzoni-Leduc [a], T. Pardoen [b], T.J. Massart [a,*]

[a] Université Libre de Bruxelles (U.L.B.), Building, Architecture & Town Planning Department (BATir), CP 194/02, Avenue F.D. Roosevelt 50, 1050 Bruxelles, Belgium
[b] Université catholique de Louvain, Department of Materials and Processes Sciences, Place Sainte Barbe, 2, B-1348 Louvain-la-Neuve, Belgium

ARTICLE INFO

Article history:
Received 30 January 2008
Received in revised form 15 May 2008
Available online 6 June 2008

Keywords:
Strain induced martensitic transformation
TRIP-assisted steels
Strain gradient plasticity
Computational homogenization

ABSTRACT

"To what extent do plastic strain gradients affect the strengthening resulting from the transformation of small metastable inclusions into hard inclusions within a plastically deforming matrix?" is the central question addressed here. Though general in the approach, the focus is on the behavior of TRIP-assisted multiphase steels. A two-dimensional embedded cell model of a simplified microstructure composed of a single metastable austenitic inclusion surrounded by a soft ferritic matrix is considered. The cell is inserted in a large homogenized medium. The transformation of a fraction of the austenite into a hard martensite plate is simulated, accounting for a transformation strain, and leading to complex elastic and plastic accommodation. The size of a transforming plate in real multiphase steels is typically between 0.1 and 2 μm, a range of size in which plastic strain gradient effects are expected to play a major role. The single parameter version of the Fleck–Hutchinson strain gradient plasticity theory is used to describe the plasticity in the austenite, ferrite and martensite phases. The higher order boundary conditions imposed on the plastic flow have a large impact on the predicted strengthening. Using realistic values of the intrinsic length parameter setting the scale at which the gradients effects have an influence leads to a noticeable increase of the strengthening on top of the increase due to the transformation of a volume fraction of the retained austenite. The geometrical parameters such as the volume fraction of retained austenite and of the transforming zone also bring significant strengthening. Strain gradient effects also significantly affect the stress state inside the martensite plate during and after transformation with a potential impact on the damage resistance of these steels.

1. Introduction

Over the last 10 years, the interest devoted to size effects in plastically deforming metals has been tremendous, motivated by the development of different engineering areas related to micro and nano-systems and to the processing of fine grained alloys. The focus has been primarily placed on measuring and modeling size effects in the response of small structures loaded homogeneously such as thin films (Nicola et al., 2003; Fredriksson and Gudmundson, 2005; Siska et al., 2007; Huang, 2007; André et al., 2007; Keralavarma and Benzerga, 2007), micropillars (Uchic et al., 2004; Tang et al., 2007) or to the response under large plastic strain gradients as promoted by nanoindentation (Delincé et al., 2006; Kizler and Schmauder, 2007; Chen et al., 2007; Abu Al-Rub, 2007), microbending (Stölken and Evans, 1998), wire torsion (Fleck et al., 1994), or the presence of

* Corresponding author. Tel.: +32 2 650 2742; fax: +32 2 650 2789.
E-mail address: thmassar@batir.ulb.ac.be (T.J. Massart).

0020-7683/$ - see front matter © 2008 Elsevier Ltd. All rights reserved.
doi:10.1016/j.ijsolstr.2008.05.025

grain boundaries or phase boundaries (Evers et al., 2004; Balint et al., 2006; Janssen et al., 2006; Yang and Vehoff, 2007; Aifantis and Ngan, 2007; Liu et al., 2007; Ekh et al., 2007). Nevertheless, one important set of problems has not yet received much attention: the size-dependent mechanics of phase transformation. Many examples of phase transformations involve large transformation strains associated to very small scale transforming features: nanometer sized precipitates in Al alloys (e.g., Radmilovic et al., 1999), martensitic transformation (e.g., Jacques, 2004), or carbide precipitation in steels (e.g., Wei et al., 2007). Other examples such as twinning can also be perceived as similar to a phase transformation often occurring at the submicron scale. Phase transformation takes place either during materials processing, especially during thermal treatments, or, dynamically, under loading. The mechanics of phase transformation directly affects the phase transformation kinetics, the development of internal stresses and the accumulation of dislocations around the transformed region (Jacques, 2004). In the case of dynamic transformation, this leads to extra hardening and strain hardening contributions. Based on the current understanding of strain gradient plasticity theory and discrete dislocation-based modeling, it can be anticipated that plastic strain gradient effects can play a prominent role in controlling phase transformation kinetics of submicron scale elements and in affecting the impact of mechanically induced phase transformation on the overall flow behavior.

In multiphase steels the interplay of hard and soft phases results in properties improvements related to a composite type response. The multiphase effect can also be enhanced owing to the stabilization by heat treatment of a residual austenitic phase: under mechanical loading the metastable austenite transforms into the harder martensitic phase. This so-called TRIP effect induces an extra strengthening contribution through three mechanisms (e.g., Fischer and Reisner, 1998; Fischer et al., 2000; Furnémont, 2003; Lani et al., 2007):

- the increase of the volume fraction of the harder martensitic phase contributing to an elevation of the global hardening through a composite type effect;
- the generation of extra dislocations around the transformed regions required to accommodate the relatively large transformation strain occurring in the transforming zone;
- the appearance of a new boundary impenetrable to dislocations leading during further deformation to an extra hardening of a region surrounding the transforming zone of the material through an higher order type effect.

The composite type effect is supposed to be coupled to the change of plastic confinement as a consequence of the growth of the martensitic region. Typical TRIP steels have austenitic grains size on the order of 1 μm with extremely good strength versus ductility balance resulting from excellent strain hardening capacity (e.g., Van Rompaey et al., 2006; Jacques et al., 2007). Several investigations have reported that smaller grain size tend to increase the stability of the austenite in fully austenitic steels (Jimenez-Melero et al., 2007). It is well admitted nowadays that for such small sizes (e.g., Fleck and Hutchinson, 1997; Fleck et al., 2003; Ma et al., 2006), geometrically necessary dislocations, required to accommodate the mismatch of properties and shape change as well as the appearance of an interface impenetrable to dislocations, will dominate the statistically stored dislocations. As a result, strain gradient effects can significantly affect the response leading to an additional strengthening contribution.

This work aims at improving the understanding of the mechanics of multiphase TRIP steels which has already received much attention in terms of numerical multi-scale cell calculations (e.g., Marketz and Fischer, 1995; Serri et al., 2005; Van Rompaey et al., 2006; Turteltaub and Suiker, 2006; Dan et al., 2007b; Tjahjanto et al., 2007; Dan et al., 2008) and constitutive model developments, (e.g., Reisner et al., 1998; Iwamoto and Tsuta, 2000; Fischer et al., 2000; Papatriantafillou et al., 2006; Dan et al., 2007a; Lani et al., 2007; Delannay et al., 2008). Among others, cell calculations have shown that within classical plasticity theory the main contribution of the TRIP effect originates from the composite effect, a conclusion that will be challenged here. To the best of the authors' knowledge, the only study addressing size effects in TRIP steels is by Turteltaub and coworkers (Turteltaub and Suiker, 2006) where the grain size effect is included in the model formulation.

In order to estimate the contribution of strain gradient plasticity effects through finite elements simulations, many strain theories are available in the literature. A first class of theories was proposed by Fleck and Hutchinson (1997), involving the gradients of the complete strain tensor in the formulation. It can be seen as an extension of Toupin and Mindlin higher order theories to the plastic regime (Toupin, 1962; Mindlin, 1964). Although this theory is adapted to account for size effects, the computational framework is complex since it requires the use of C^1 interpolation for the displacement field or the use of two independent interpolations for the strain gradient tensor and the displacement field with a penalty-enhanced C^0 interpolation.

In a second class of theory, the strain gradient effects are included in the plastic regime only. In de Borst and Mühlhaus (1992) and de Borst and Pamin (1996), strain gradients enter the yield condition, requiring the same interpolation scheme as in previous works: C^1 or penalty-enhanced C^0 interpolation fields. Fleck and Hutchinson (2001) proposed to include the gradient effects within a generalized higher order field equation, which is only activated in the plastic regime, and within a generalized effective plastic strain measure. It provides a simplified version of the former Fleck and Hutchinson (1997) higher order theory, while preserving the key ingredients to predict size effects (Niordson and Hutchinson, 2003b; Engelen et al., 2006). A simple case of this theory can be used to recover the initial Aifantis theory (Aifantis, 1984). A straightforward C^0 implementation scheme is proposed in Niordson and Hutchinson (2003b) where the displacement rate and the effective plastic strain rate are treated as unknowns on equal footing. Yet, the restriction on the validity of the higher order field equation is a disadvantage of using this theory: indeed, boundary conditions need to be specified at the internal and continuously moving elasto-plastic boundary. The consequences of this aspect have been recently treated in the literature (Niordson and Hutchinson, 2003b; Gudmundson, 2004; Polizzotto, 2007; Peerlings, 2007).

Non-local theories constitute a third class of interest, usually adapted for the study of softening and localization (e.g., Engelen et al., 2006). The framework elaborated by Engelen et al. (2006) was shown to be less adapted to size effects in hardening materials. The framework proposed by Peerlings (2007) is more complete regarding the detailed treatment at the moving elasto–plastic boundaries: it more rigourously clarifies the proper boundary conditions to apply at the moving elasto-plastic boundary. The current version is, however, only applicable to linear hardening.

As a result, the theory of Fleck and Hutchinson (2001) has been selected as a good trade off between simplicity and relevance for the present problem and implemented within a finite element code in order to investigate the size effects resulting from the TRIP mechanism.

The outline of the paper is the following. Section 2 describes the physical model, i.e., the microstructure idealization, the phase transformation and the loading conditions while Section 3 introduces the mechanical description of the different phases, and the strain gradient plasticity theory. A parameter study of a simplified microstructure is presented in Section 4 with a specific attention to the influence of (i) the boundary conditions on plastic flow at the elasto–plastic boundaries, (ii) the intrinsic length parameter, (iii) the geometrical parameters such as the volume fraction of retained austenite and of the transforming zone, (iv) the overall strain $E^{\text{start}}_{\text{tsf}}$ at which transformation is assumed to start. The results obtained in Section 4 are discussed in Section 5 while opening to wider perspectives in terms of material properties optimization.

2. Phase transformation modeling

Since the retained austenitic phase is metastable at room temperature, it can transform under straining into the harder martensitic phase by successive bursts. In the next subsection, the phase transformation mechanisms are described together with the microstructure. The following notations, classical in physical metallurgy, will be used:

$\alpha \rightarrow$ ferrite, $\alpha' \rightarrow$ martensite,
$\gamma \rightarrow$ austenite, HOM $\rightarrow$ homogenized medium.

2.1. Physical model for the transformation of a retained austenite inclusion

The simplified representative microstructure described in Fig. 1a will be treated in two dimensions, under plane strain tensile loading conditions. It is composed of a cylindrical austenitic inclusion surrounded by a ferritic matrix. In the case of uniaxial loading, it has been shown that the martensitic variant maximizing the mechanical driving force, and thus the most susceptible to transform, is the closest to the 45° angle with respect to the tensile axis (Van Rompaey et al., 2006), which corresponds to the *x*-axis here. Moreover, an elliptical transforming zone is chosen in this work in order to avoid stress singularities at the tips of the transforming region which might lead to overestimating the gradients effects. The volume fraction of the transforming zone is in principle controlled by the phase transformation condition, which is, in turn, directly affected by the microstructure geometric confinement and the balance of driving forces and resistive forces. Modeling explicitly the nucleation and growth of the martensitic phase in this system is extremely complex and remains a question of debate, especially regarding nucleation. It lies outside the scope of this study, see contributions by Weschler et al. (1953), Olson and Cohen (1975), Leblond et al. (1986), Ball and James (1987), Stringfellow et al. (1992), Bhattacharya (1993), Diani et al. (1995), Tomita and Iwamoto (1995), Levitas and Stein (1997), Cherkaoui et al. (1998), Ganghoffer and Simonsson (1998), Levitas et al. (1998a), Levitas (1998b), Fischer and Reisner (1998), Reisner et al. (1998) and Fischer et al. (2000). Here, the final volume of the martensitic zone is imposed in the simulation and the transformation is assumed to occur homogeneously within the lenticular plate. The volume fraction of the lenticular plate is imposed to vary between 0% and 6%, which corresponds to realistic values, see (Jacques, 2004). Note that other plates will usually transform later in the deformation process, which is not modeled here, see Marketz and Fischer (1995). The stress-free transformation strain involves a shear component γ^{tsf} and a dilatation component δ^{tsf} along the small axis of the plate, and has the following form in the local axis (1,2) of the lenticular plate, see Fig. 1b:

$$\varepsilon^{\text{tsf}}_{\text{loc}} = \begin{bmatrix} 0 & 0 & 0 \\ 0 & 0 & \gamma^{\text{tsf}}/2 \\ 0 & \gamma^{\text{tsf}}/2 & \delta^{\text{tsf}} \end{bmatrix}. \tag{1}$$

The deformation process is modeled in three stages:

- The cell is first deformed until the overall strain E reaches the strain prescribed for the onset of transformation. This value $E^{\text{start}}_{\text{tsf}}$ corresponds to an average strain $\langle\epsilon\rangle^{\text{start}}_{\text{tsf},\gamma}$ in the austenite. Since the strength mismatch is not very large between austenite and ferrite, $\langle\epsilon\rangle^{\text{start}}_{\text{tsf},\gamma}$ will not differ too much from $E^{\text{start}}_{\text{tsf}}$. The corresponding overall stress Σ is noted $\Sigma^{\text{start}}_{\text{tsf}}$.
- An artificial thermal loading stage is then applied: a variation of temperature ΔT associated to fictitious thermal expansion coefficients α_{ij} allows imposing the transformation strain $\varepsilon^{\text{tsf}}_{\text{loc}}$ to the prescribed transforming region. The material properties are also changed following a linear variation with ΔT. As a result, the transformation is assumed to occur at constant macroscopic strain $E^{\text{start}}_{\text{tsf}}$ or macroscopic stress $\Sigma^{\text{start}}_{\text{tsf}}$.
- The thermal loading ends and the mechanical loading is resumed.

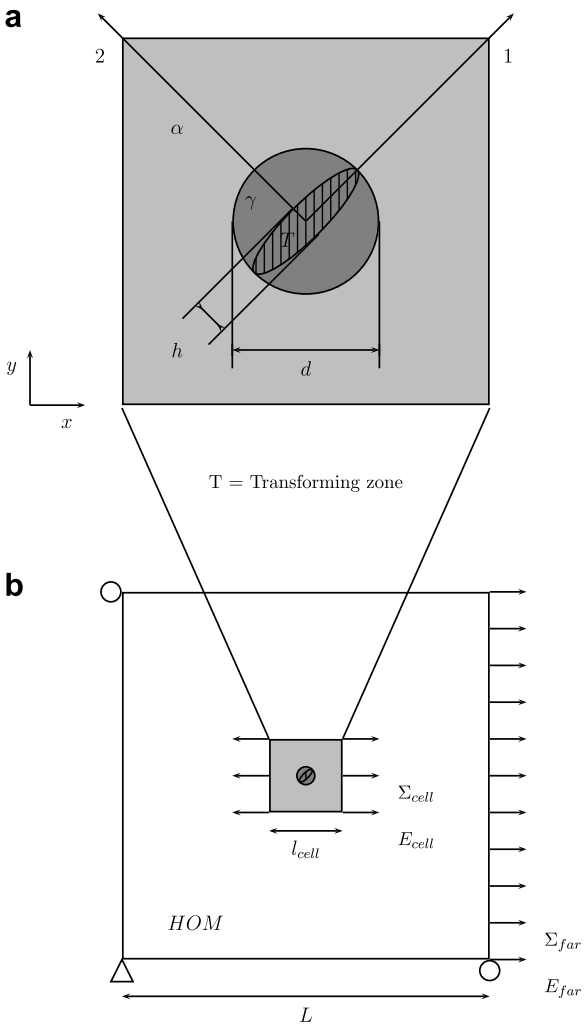

Fig. 1. Simplified microstructure: (a) geometrical parameters; (b) embedded cell model.

2.2. Embedded cell model

There are two extreme ways to control the loading of the unit cell during the phase transformation by keeping either the average stress Σ constant and equal to $\Sigma_{\text{tsf}}^{\text{start}}$ or the average strain E constant and equal to $E_{\text{tsf}}^{\text{start}}$. These quantities can be controlled from boundary tractions or displacements on the unit cell (e.g., Kouznetsova et al., 2001). For the sake of illustration, Fig. 2 shows the response of a unit cell calculation (as described later in Section 4) with transformation occurring under either load or displacement control. Obviously, the boundary conditions have a strong impact on the response, at least during the transient regime following the transformation, which makes this simple unit cell model unadapted. An embedded cell model has been considered in order to make the transformation stage independent of the mechanical control on the cell, see also Van Rompaey et al. (2006). As shown in Fig. 1a the unit cell is embedded in a surrounding composite with the same uniaxial behavior as the one obtained by averaging the behavior of a non-transforming unit cell. This allows the transformation behavior to be independent of the mechanical control on the cell provided the ratio $\frac{l_{\text{cell}}}{L}$, see Fig. 1b, is sufficiently small: typically a ratio smaller than $\frac{1}{5}$ is advised in the literature, see Dong and Schmauder (1996). Fig. 2 shows that the response of the embedded cell model (with $\frac{l_{\text{cell}}}{L} = 1/6$) is intermediate between the two extreme behaviors of the unit cell model, under constant Σ or E. The response of the transforming unit cell is then obtained by averaging the stress and strain over the volume of the representative central unit cell:

$$E_{\text{cell}} = \frac{1}{V_{\text{cell}}} \int_{V_{\text{cell}}} \varepsilon \, \mathrm{d}V_{\text{cell}},$$
$$\Sigma_{\text{cell}} = \frac{1}{V_{\text{cell}}} \int_{V_{\text{cell}}} \sigma \, \mathrm{d}V_{\text{cell}}. \tag{2}$$

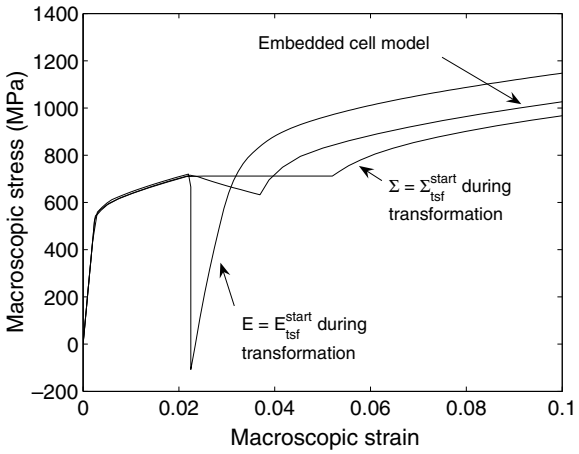

Fig. 2. Influence of mechanical boundary conditions on the overall stress/strain curve along the tensile direction – l_*/d=1 and unconstrained plastic flow at elasto-plastic boundaries.

A uniform horizontal displacement U_x is applied on the boundary of the surrounding composite, while leaving free the boundary transverse to the y-axis leading to overall uniaxial tension conditions (Fig. 1b).

Note that during the transient regime, significant unloading takes place in the unit cell resulting mostly from the dilatation component of the transformation strain. This important feature of the TRIP process will be addressed in detail in this paper.

3. Strain gradient plasticity theory

3.1. The generalized effective plastic strain rate

In this section, the essentials of the Fleck and Hutchinson (2001) strain gradient plasticity theory are summarized. As in classical plasticity theories, the higher order theory is based on the usual definition of the conventional effective plastic strain rate $\dot{\epsilon}_{\mathrm{P}}$:

$$\dot{\epsilon}_{\mathrm{P}} = \sqrt{2\dot{\epsilon}^{\mathrm{P}}_{ij}\dot{\epsilon}^{\mathrm{P}}_{ij}/3}. \tag{3}$$

The von Mises effective stress is expressed as $\sigma_{\mathrm{e}} = \sqrt{\frac{3}{2}s_{ij}s_{ij}}$, where s_{ij} is the deviatoric part of the Cauchy stress tensor. The direction of the plastic strain increment is defined as $m_{ij} = 3s_{ij}/2\sigma_{\mathrm{e}}$ and the plastic strain rate tensor is expressed as: $\dot{\epsilon}^{\mathrm{P}}_{ij} = \dot{\epsilon}_{\mathrm{P}} m_{ij}$. In order to introduce higher order terms in the formulation, a generalized effective plastic strain rate is defined, including gradients of effective plastic strain rate and up to three length parameters setting the scale at which gradients effects are important. In the simple case of a single length plastic strain gradient theory, the definition of the generalized effective plastic strain rate is given by:

$$\dot{E}^2_{\mathrm{P}} = \dot{\epsilon}^2_{\mathrm{P}} + l^2_* \dot{\epsilon}_{\mathrm{P},i}\dot{\epsilon}_{\mathrm{P},i} \tag{4}$$

which leads to a theory resembling the one proposed initially by Aifantis (1984).

In the implementation proposed by Niordson and Hutchinson (2003b), this single parameter theory is used with a C^0 interpolation of the displacement field and of the plastic strain rates. It retains the essential ingredients of the original Fleck and Hutchinson (2001) theory since it involves the higher order terms. However, the influence of the plastic flow direction gradient $m_{ij,k}$ is neglected in the definition of generalized effective plastic strain rate. This leads to an aggregate effect of plastic gradients without separating extensional and rotational effects, which has already been shown to decrease the magnitude of the size effects in specific loading configurations (see Niordson and Hutchinson, 2003b).

3.2. Governing and constitutive equations

The Fleck and Hutchinson (2001) theory is a generalization of the classical J_2 flow theory. The principle of incremental virtual work can be stated as follows, for each displacement and effective plastic strain rates:

$$\begin{aligned} &\forall \delta\dot{u}_i, \quad \forall \delta\dot{\epsilon}_{\mathrm{P}} \\ &\int_V \left\{ \dot{\sigma}_{ij}(\delta\dot{\epsilon}^{\mathrm{e}}_{ij} + \delta\dot{\epsilon}^{*}_{ij}) + \dot{Q}\delta\dot{\epsilon}_{\mathrm{P}} + \dot{\tau}_i \delta\dot{\epsilon}_{\mathrm{P},i} \right\} \mathrm{d}V = \int_S \left(\dot{T}_i \delta\dot{u}_i + \dot{t}\delta\dot{\epsilon}_{\mathrm{P}} \right) \mathrm{d}S, \end{aligned} \tag{5}$$

where a transformation strain ϵ^*_{ij}, being non-zero only in the transforming zone, is introduced. Q is the generalized effective stress, work conjugate to the plastic strain ϵ_P and τ_i is the higher order stress which is the work conjugate to the gradient of the effective plastic strain. In the absence of body forces, straightforward manipulations lead to the corresponding strong form of the field equations:

$$\dot{\sigma}_{ij,j} = 0 \tag{6}$$

which is the equilibrium equation, and

$$\dot{\sigma}_e = \dot{Q} - \dot{\tau}_{i,i} \tag{7}$$

which is a generalized field consistency equation only valid in the plastic regime, together with associated boundary conditions

$$\begin{aligned} \dot{T}_i &= \dot{\sigma}_{ij} n_j, \\ \dot{t} &= \dot{\tau}_i n_i. \end{aligned} \tag{8}$$

To close the formulation, the incremental constitutive equations are given by:

$$\begin{aligned} \dot{\sigma}_{ij} &= L_{ijkl}(\dot{\epsilon}_{kl} - \dot{\epsilon}^P m_{kl} - \dot{\epsilon}^*_{kl}), \\ \dot{\tau}_i &= h(E_P)(l_*^2 \dot{\epsilon}_{P,i}), \\ \dot{Q} &= h(E_P)(\dot{\epsilon}_P), \end{aligned} \tag{9}$$

where L_{ijkl} denotes the elastic stiffness tensor for an isotropic solid and h is the hardening function which is defined by:

$$h = \left.\frac{\mathrm{d}\sigma_y(\kappa)}{\mathrm{d}\kappa}\right|_{E_P}, \tag{10}$$

where $\sigma_y(\kappa)$ is the hardening law, κ is the hardening parameter measuring the accumulation of dislocations. Hardening is evaluated at $\kappa = E_P$ rather than at $\kappa = \epsilon_P$ to take into account the contribution of the geometrically necessary dislocations associated to the plastic gradients. The consistency equation governing plastic flow is now expressed through the generalized effective stress by $Q = Q_y$ where the evolution of Q_y is given by:

$$\dot{Q}_y = h(E_P)(\dot{\epsilon}_P). \tag{11}$$

3.3. Implementation issues

In this study, an implementation of the theory similar to the one presented in Niordson and Hutchinson (2003b) is used. The implementation is purely incremental, equilibrium is not enforced through the successive iterations. Small time steps are therefore used to minimize the divergence to the exact solution. The convergence with respect to time step and mesh refinement has been carefully checked. A mesh containing 11,744 elements has been used for generating the results presented here. The displacement rate and the effective plastic strain rate are treated as two independent unknowns on equal footing. A bi-quadratic interpolation is used for the displacement rate, and a bi-linear interpolation is used for the effective plastic strain rate in order to ensure similar variations in the calculation of the total strain rate. The elasto–plastic transition is tested at each Gauss point: if the von Mises equivalent stress at a Gauss point in the elastic domain becomes larger than the yield stress, the Gauss point is considered to enter the plastic regime. Elastic unloading occurs whenever the effective plastic strain rate calculated at a plastic Gauss point is negative (see Niordson and Hutchinson, 2003b). As mentioned earlier, the theory is implemented using an independent effective plastic strain rate field. As a result, higher order boundary conditions must be specified at the external boundary of a region where plastic flow occurs. Two extreme types of conditions can be considered (Niordson and Hutchinson, 2003b):

- At a free surface, dislocations pass through unimpeded. No constraint on the effective plastic strain rate $\dot{\epsilon}_P$ should then be applied, which is equivalent to the natural boundary condition on the higher order traction, i.e., $\dot{\tau}_i n_i = 0$.
- At a strongly bonded interface, or an interface between phases, dislocations cannot cross the interface and accumulate in the near interface region. The essential boundary condition corresponding to a boundary impenetrable to dislocations is $\dot{\epsilon}_P = 0$.

The incremental nature of the Fleck and Hutchinson (2001) theory is well adapted to study the phase transformation. It allows accounting for the evolving nature of the interface between austenite and martensite, which does not exist before transformation and becomes impenetrable to dislocations. The plastic flow is suddenly constrained along the interface by setting the rate of effective plastic strain equal to zero, i.e., $\dot{\epsilon}_P = 0$ at the onset of the transformation.

Finally, boundary conditions must be given along the elasto–plastic boundary region. Again the two choices of boundary conditions described above are possible at elasto–plastic boundaries. The choice is not so obvious, (e.g., Peerlings, 2007), although the physics calls more for the natural boundary condition $\dot{\tau}_i n_i = 0$.

4. Parameter study

A study of the effect of the main parameters of the problem is performed with the embedded cell model described in Section 2. This section starts with the selection of parameters variations. Then, the influence of the boundary conditions on the plastic flow at the elasto–plastic boundary is analyzed. Finally, the effect of plastic strain gradients is systematically studied by varying the main parameters affecting the martensitic transformation.

4.1. Selection of material parameters and model parameters

All the phases are assumed to follow a Swift-type hardening law

$$\sigma_y = \sigma_{y_0}(1 + h_0\kappa)^n, \tag{12}$$

where σ_y is the current yield stress, σ_{y_0} is the initial yield stress, h_0 is the hardening coefficient, n is the strain hardening exponent and κ is the hardening parameter (evaluated at $\kappa = E_P$ as explained previously).

In order to make the simulation realistic, the flow parameters used for each phases are motivated from previous experimental and modeling efforts on a specific grade of TRIP-assisted multiphase steels (Furnémont, 2003). These parameters are collected in Table 1. In addition to the elastic and plastic behavior of the phases, some of the parameters related to the transformation are kept fixed in this study:

- the longitudinal transformation strain along the small axis of the lenticular plate δ^{tsf} is set equal to 3%;
- the shear component of the transformation strain γ^{tsf} is taken equal to 20% as usual.

The parameters varied in the study are:

- the volume fraction of the transforming zone with respect to the initial austenitic inclusion quantified by h/d varying between 0 and $1/3$, where h is the width of the lenticular plate and d is the diameter of the inclusion as shown in Fig. 1a;
- the volume fraction of retained austenite f_γ with respect to the global distribution of phases varying between 0% and 20%;
- the intrinsic length parameter, l_*, normalized by the diameter of the inclusion d, i.e., l_*/d varying between 0 and 2;
- the macroscopic strain level E_{tsf}^{start} at which transformation starts varying between 0% and 4.4%.

Four cases are considered:

- *Case No. 1:* No phase transformation occurs, corresponding to the response of a composite cell ferritic matrix/austenitic inclusion.
- *Case No. 2:* A change of elasto-plastic properties occurs in the transforming region accompanied by evolutive boundary conditions: the plastic flow is unconstrained during the first stage and becomes constrained during stages 2 and 3 at the austenite–martensite interface to represent the new impenetrable phase boundary.
- *Case No. 3:* The transformation strain is applied on top of the change of elasto–plastic behavior and the evolutive boundary conditions at the austenite–martensite boundary as specified in Case No. 2.
- *Case No. 4:* The transformation strain only is applied to the unit cell without any modification of the elasto–plastic properties of the transforming region and thus without any evolving boundary conditions on plastic flow at the interface of the transformed region.

The stress–strain response associated to the embedded cell presented in Fig. 1a is computed from the averaging of the microstresses and microstrains over the volume of the unit cell using Eq. (2). The contribution of the transformation to the strengthening is described through an indicator $S(E)$ which is defined at a given macrostrain E as:

$$S(E) = \frac{\Sigma}{\Sigma_{ref}} \tag{13}$$

where Σ_{ref} is the average stress corresponding to the average strain E on the stress–strain curve obtained in Case No. 1, and Σ corresponds to the average strain E in either Cases No. 2, No. 3 or No. 4.

Table 1
Material parameters

	Ferrite	Austenite	Martensite
E (GPa)	200	187	200
σ_{y_0}(MPa)	475	700	2000
h_0	55	50	800
N	0.27	0.3	0.05

4.2. Preliminary study: general picture without size effect

In order to set the stage for the rest of the analysis, results obtained for the specific set of parameters $f_\gamma = 20\%$, $h/d = 1/3$, $l_*/d = 0$, $E_{\text{tsf}}^{\text{start}} = 2.25\%$ are first given without introducing any size effects in order to briefly recall the key phenomena playing a role in the mechanics of the TRIP effect. The overall volume fraction of the transforming zone is equal to only 3%. Fig. 3 shows the stress–strain curve obtained in Cases No. 1, No. 2 or No. 3 with the use of the classical J_2 plasticity theory. After the transient, the two curves corresponding to Cases No. 2 and No. 3 match each other, showing that most of the strengthening associated to the TRIP effect results from a composite type effect, i.e., comes from the introduction of a hard phase into a softer matrix. The absence of strengthening contribution associated to the transformation strain might partly come from the fact that the transient stage is not yet terminated at $E = 15\%$ (see further). Note that the TRIP contribution is apparently relatively small in terms of yield stress increase, even though significant enough in terms of the increase of the strain hardening capacity to slightly improve both the tensile strength and the uniform elongation. This is a first indication that without introducing strain gradient plasticity effects it is hard to see how reconciling these results with the huge effects observed in the experiments (Jacques, 2004).

The repartition of the equivalent von Mises stress σ_{e} and the equivalent strain ε_{P} are shown in Fig. 4a and b when the macroscopic tensile strain reaches 5.5% in Case No. 3. The transformation strain and the change of plastic confinement are accommodated by the plastic flow around the transforming zone resulting in significant plastic strain gradients in the matrix and in the austenitic phase. A strong concentration of the equivalent stress is also detected around the lenticular plate which is undergoing a large compressive stress state.

Fig. 5a depicts the average behavior of the three phases in terms of phase averaged microstresses $\langle\sigma\rangle$ and microstrains $\langle\epsilon\rangle$ along the tensile loading direction. The transforming zone undergoes large compressive stresses during transformation due to the dilatation component of the transformation strain. Fig. 5b shows the variation during the transformation of the phase averaged microstresses $\langle\sigma\rangle$ as a function of the macroscopic strain E in the main loading direction. A state of tensile stress is recovered only after 4.5% macroscopic strain in the martensitic transforming region. The austenitic and ferritic phases are subjected to a shorter transient stage.

4.3. Influence of the boundary conditions at the elasto-plastic boundary

The results of simulations obtained using $f_\gamma = 10\%$, $h/d = 1/3$, $E_{\text{tsf}}^{\text{start}} = 2.25\%$, are now reported for the case where the intrinsic length parameter is on the order of the microstructure representative dimension, i.e., $l_*/d = 1$, using the strain gradient plasticity theory presented in Section 3. The two possible boundary conditions on the plastic flow at the elasto-plastic boundaries, except at the martensitic/austenitic interface (which is always constrained in Cases No. 2, No. 3 as from stage 2), are considered: the plastic flow is either constrained by the essential condition $\dot{\epsilon}_{\text{P}} = 0$ or unconstrained; i.e., by applying $\dot{\tau}_i n_i = 0$. Fig. 6a shows the stress–strain curves obtained in the case of constrained plastic flow at every elasto-plastic boundaries for Cases No. 2 and No. 3. A 20% increase of the strengthening is observed at the end of the computation if only the elasto-plastic properties are changed during the transformation (Case No. 2) whereas adding the effect of the transformation strain (Case No. 3) leads to more than 40% increase of the flow stress with respect to the reference curve. Fig. 6b presents the set of curves corresponding to the unconstrained plastic flow at the elasto-plastic boundaries. The strengthening brought about by the change of material properties (Case No. 2) is significant in this case too and of the same order of magnitude

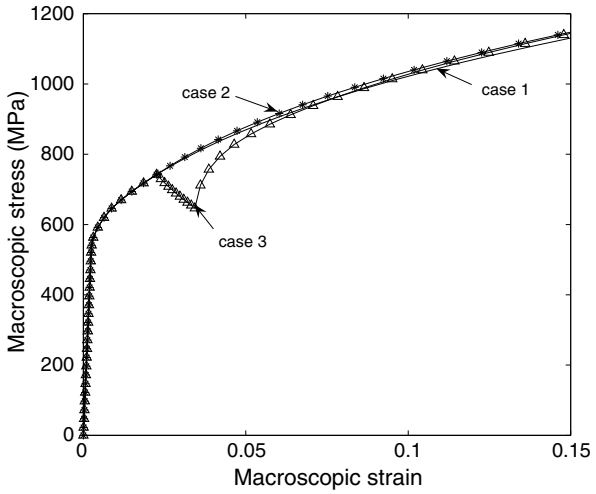

Fig. 3. Stress-strain response along the tensile direction of the embedded cell without size effects, using $f_\gamma = 20\%$, $h/d = 1/3$, l_*/d=0, $E_{\text{tsf}}^{\text{start}} = 2.25\%$ in Cases No. 1, No. 2 and No. 3.

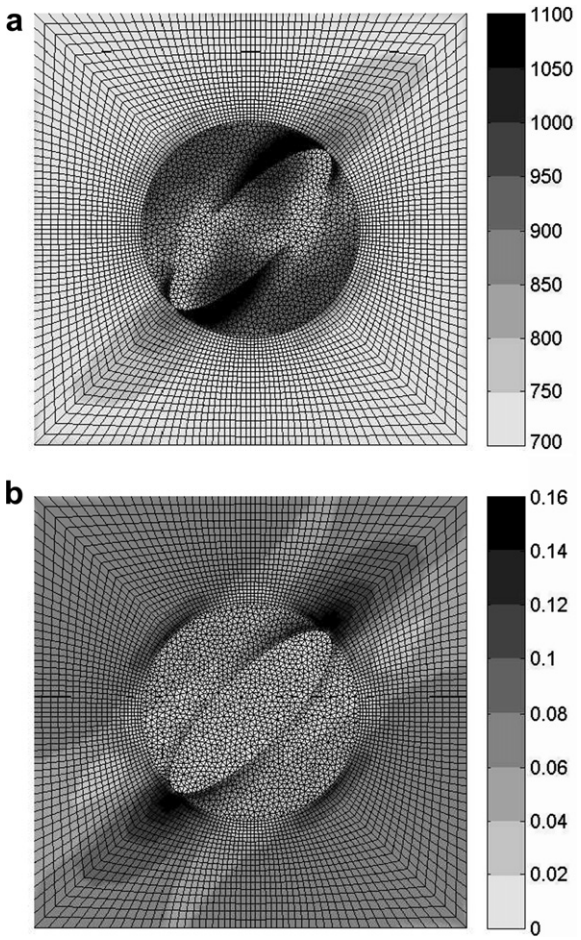

Fig. 4. (a) Equivalent von Mises stress (MPa) and (b) equivalent plastic strain distributions at $E = 5.5\%$ using $f_\gamma = 20\%$, $h/d = 1/3$, l_*/d=0, $E_{\text{tsf}}^{\text{start}} = 2.25\%$ in Case No. 3.

as the one obtained in Fig. 6a. As shown in Fig. 6b, adding the transformation strain induces a marginal enhancement of the overall strengthening when plastic flow is unconstrained at elasto–plastic boundaries. This strong difference between the curves corresponding to Case No. 3 in Fig. 6b and a is directly linked to the presence of elastically unloading regions in the ferritic phase and will be clarified in the discussion presented in Section 5.

Constraining the plastic flow at every elasto–plastic boundaries can be considered as giving an upper bound of the strengthening that can be expected from the TRIP mechanism, while a lower bound is obtained when the plastic flow is unconstrained at elasto–plastic boundaries (except again at the austenitic/martensitic interface). The last condition is presumably the most physical and will be used for the rest of the paper, at least to provide conservative results.

4.3.1. Influence of the intrinsic length

Fig. 7 shows the stress/strain curves corresponding to $l_*/d = 0, 0.5, 1$ and 2 for Case No. 3. The value of the intrinsic length parameter and associated strain gradient plasticity effects and the higher order boundary condition at martensitic/austenitic interface have a major impact on the strengthening, due to significant strain gradients in the matrix and in the residual austenite accommodating the transformation energy and the presence of a hard inclusion.

Fig. 8a shows the variation of the strengthening indicator S as a function of the intrinsic length parameter l_*/d at a strain $E_{\text{macro}} = 4\%$, which corresponds to the transient regime: the martensite is still undergoing high compression at this strain level. As a result, the strengthening indicator is smaller than 1 in Case No. 4, and is higher in Case No. 2 compared to Case No. 3. At $E_{\text{macro}} = 8\%$, the picture is different (Fig. 8b): a specific contribution of the stress free transformation strain on top of the change of flow properties is noticeable if l_*/d ranges between 0.1 and 1. On the contrary, when l_*/d is larger than 1, the transformation strain has a negative impact on the strengthening. This is due to the fact that the unit cell is still in the transient regime. A finite strain formulation of the theory would be needed to generate results valid at larger strains.

Fig. 9a and b depict the evolution of, respectively, the phase averaged stress $\langle \sigma_{\alpha'} \rangle$ along the tensile loading direction as a function of the phase averaged strain $\langle \epsilon_{\alpha'} \rangle$ and of the macroscopic strain E along the tensile loading direction in the martens-

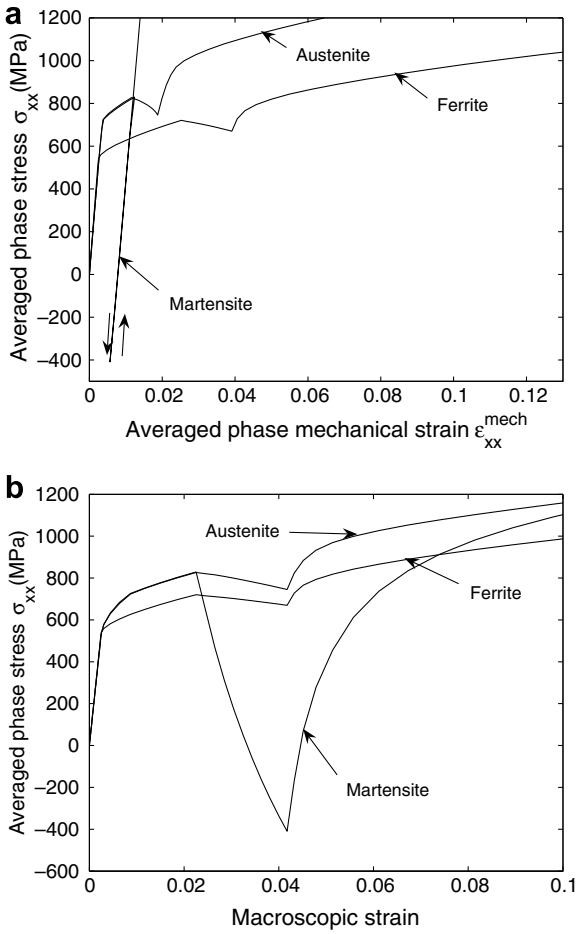

Fig. 5. Evolution of the phase averaged stress in the martensite, austenite and ferrite, without any size effect, as a function of (a) the phase averaged strain and (b) the averaged strain E using $f_\gamma = 20\%$, $h/d = 1/3$, $l_*/d = 0$, $E_{tsf}^{start} = 2.25\%$, for Case No. 3.

itic phase for Case No. 3 and for $l_*/d = 0, 0.5, 1, 2$. From Fig. 9b, it appears that increasing values of the ratio l_*/d amplifies the back stress effects associated to the transformation. The transient regime also lasts longer when l_*/d increases, i.e., it takes longer for the martensite to restart undergoing tensile stresses after transformation. The stress levels attained during compression are quite large. Note that no condition for cracking under compression nor tension is accounted for in the model.

Fig. 10a and b show the evolution of, respectively, the phase averaged stress $\langle \sigma_{\alpha'} \rangle$ as a function of the phase averaged strain $\langle \epsilon_{\alpha'} \rangle$ or of the macroscopic strain E in the martensitic phase for Case No. 2 (i.e., no transformation strain) and for $l_*/d = 0, 0.5, 1, 2$. As expected, the transient is much shorter and does not lead to any unloading inside the martensite. After the transient, the stress within the martensite reaches about 1500 MPa.

4.4. Influence of the microstructural parameters

4.4.1. Influence of the volume fraction of the transforming zone

In this subsection, the influence of the volume fraction of the transforming zone, quantified by the parameter h/d, is analyzed for h/d equal to 0, 1/6 and 1/3, corresponding to a volume fraction of the transforming zone equal to 0%, 1.5% and 3%, respectively, for Case No. 3. As expected and illustrated in Fig. 11, increasing the volume fraction of the transforming phase enhances the strengthening resulting from the TRIP effect.

4.4.2. Influence of the volume fraction of retained austenite

The volume fraction of retained austenite f_γ is varied between 0% and 20% while keeping the ratio h/d equal to 1/3. As a result, the volume fraction of the transforming phase is also varying between 0% and 6%. Fig. 12 shows that increasing f_γ obviously leads to enhanced strengthening. The evolution of S as a function of f_γ is shown in Fig. 13a and b. When $E_{macro} = 5\%$, the additional stress free transformation strain seems to have a negative impact on the hardening enhancement because the transient regime is not yet finished (compare Cases No. 2 and No. 3). The evolution of S at $E_{macro} = 8\%$ shows that

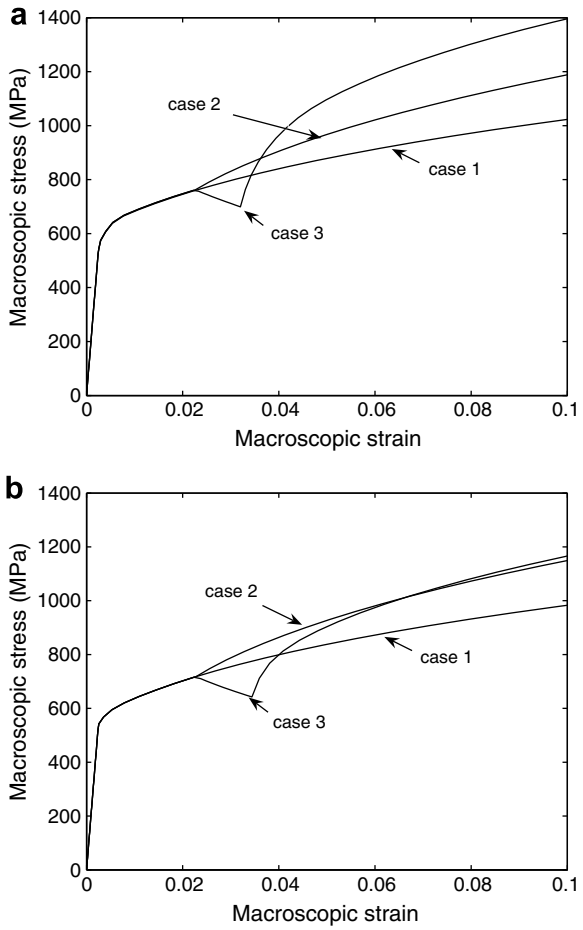

Fig. 6. Effect of the conditions applied at the elasto–plastic boundary on the overall stress strain curve along the tensile direction in the framework of the strain gradient plasticity theory, using $f_\gamma = 10\%$, $h/d = 1/3$, l_*/d=1, $E^{start}_{tsf} = 2.25\%$ (a) constrained plastic flow at elasto–plastic boundaries, (b) unconstrained plastic flow at elasto–plastic boundaries in Cases No. 1, No. 2 and No. 3. The plastic flow is always fully constrained at the α'/γ interface.

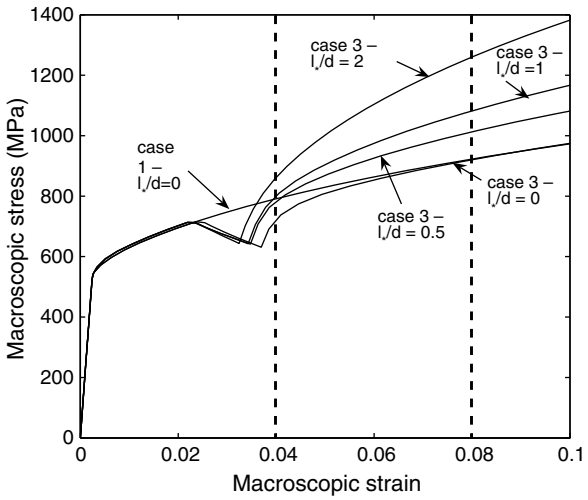

Fig. 7. Influence of the ratio l_*/d on the stress strain response along the tensile direction of the representative unit cell with constrained plastic flow at the α'/γ interface and unconstrained plastic flow at the other elasto-plastic boundaries, $f_\gamma = 10\%$, $h/d = 1/3$, $E^{start}_{tsf} = 2.25\%$ in Cases No. 1 and No. 3.

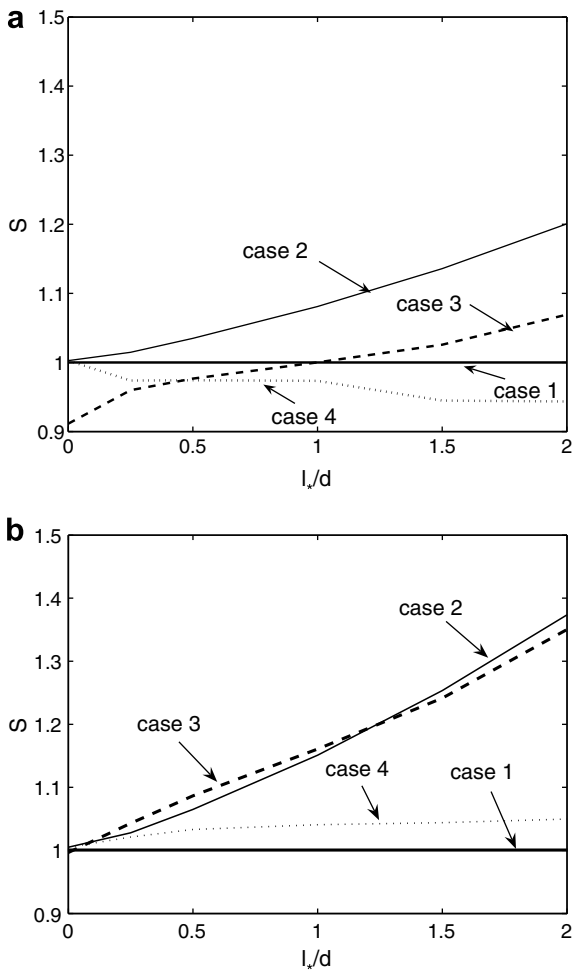

Fig. 8. Variation of the strengthening indicator S as a function of l_*/d, with constrained plastic flow at the α'/γ interface and unconstrained plastic flow at every other elasto–plastic boundaries, $f_\gamma = 10\%$, $h/d = 1/3$, $E_{tsf}^{start} = 2.25\%$ (a) at $E_{macro} = 4\%$ (b) at $E_{macro} = 8\%$, for Cases No. 1, No. 2, No. 3 and No. 4.

the transformation strain negative impact tends to attenuate when $f_\gamma > 10\%$. When $f_\gamma = 10\%$, the transformation strain has a small effect on the overall hardening. Moreover, both the volume fraction of retained austenite and of the transforming zone are varying: this leads to stronger effects than in the previous subsection.

4.4.3. Influence of the average strain at which transformation occurs E_{tsf}^{start}

Fig. 14 shows the stress/strain curves obtained when E_{tsf}^{start} is equal to 0%, 2.25% and 4.43%. The earlier the transformation starts, the shorter the transient and the larger the strengthening.

5. Discussion

5.1. Discussion about the boundary conditions

The first important result to discuss regarding the parametric study is the first order effect of the boundary conditions on the strengthening associated to the transformation of a portion of a soft inclusion into a hard plate. The focus being on the contribution to the strengthening resulting from the TRIP effect, no constraint was prescribed along the inclusion matrix interface, austenite–ferrite in the case of a multiphase TRIP steel. The austenite/ferrite interface should also, in principle, lead to an additional Hall-Petch type hardening controlled by the size of the austenite grain. The Hall-Petch contribution resulting from the ferrite/ferrite grain boundary is considered to be convoluted in the properties of the phase determined experimentally. As explained above, the interface between the hard plate (martensite) and the surrounding softer un-transformed portion of the inclusion (austenite) is always assumed impenetrable from the start of the transformation, an assumption which has a strong physical foundation: dislocations do not cross the interface between austenite and martensite.

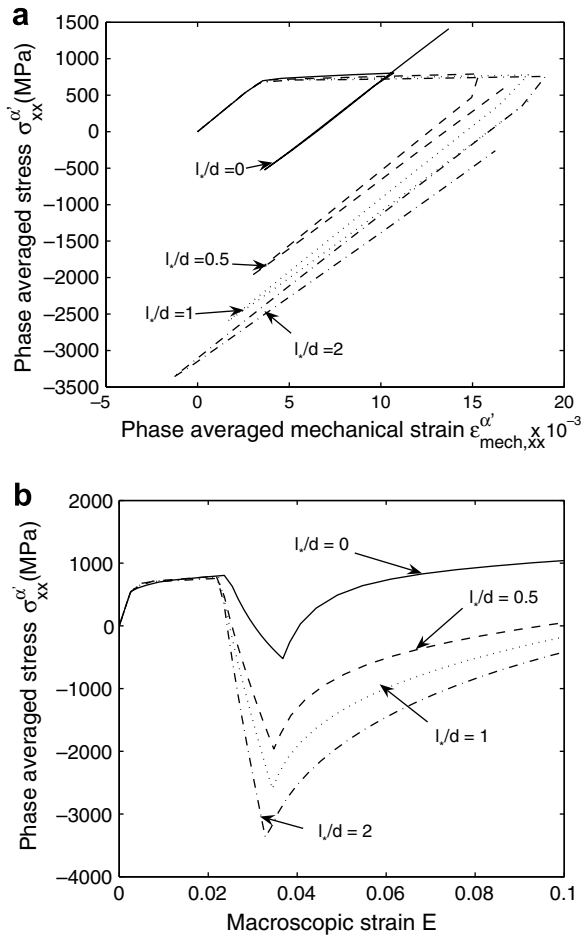

Fig. 9. Variation of the phase averaged stress in the martensite as function of (a) the phase averaged strain and (b) of the averaged strain E for various ratios l_*/d using $f_\gamma = 10\%$, $h/d = 1/3$, $E^{start}_{tsf} = 2.25\%$ and for Case No. 3.

Only the change of constraint exercised along the moving elasto-plastic boundary has been considered. When no constraint is applied at this boundary, a significant strengthening associated to the TRIP effect is observed resulting almost entirely from the change of properties of the transforming region (and from the related change of confinement) and not from the transformation strain. On the contrary, if plastic flow is constrained at the elasto-plastic boundary, an additional strengthening associated to the transformation strain of the transforming region shows up.

The comparison of Fig. 6a and b shows that the curves corresponding to Case No. 2 (modification of material properties of the transforming region without transformation strain) are almost identical for the constrained and unconstrained cases.

This specific effect of the transformation strain can be understood by analyzing the confinement of the plastic flow. The effect of plastic confinement in higher order theories is frequently illustrated using the one-dimensional example of an infinite shear layer embedded between one or two rigid substrates (Fleck and Hutchinson, 2001). The strengthening of such a layer results from the plastic flow being impeded at one or both of the interfaces between the substrates and the deforming layer. A larger strengthening is obtained when both layer boundaries are constrained (two hard substrates), instead of one (one hard substrate, and one soft substrate). The strengthening increases when the thickness of the layer decreases.

In the present case, the key point to interpret the lack of contribution of the transformation strain in the case of unconstrained plastic flow at the elasto-plastic boundaries in the ferrite and the residual austenite is related to the presence of unloading zones. These elastically unloading zones are shown in Fig. 15a and b (dark areas), for the constrained and unconstrained cases, at the end of the transformation. Note that in Fig. 15b, the martensite is partially elastic. It can be seen that for both types of conditions applied at the elasto-plastic boundary, approximately the same unloading zones are found. Note also that the boundary of the (martensitic) transforming plate is always constrained. This means that the plastically deforming zones in the constrained case are completely surrounded by impenetrable boundaries (fixed or moving) on both sides. Furthermore, these plastically deforming regions have a width on the order of the intrinsic length scale and undergo large shear strains associated to the transformation. These confined zones lead to large strengthening such as in the shear layer

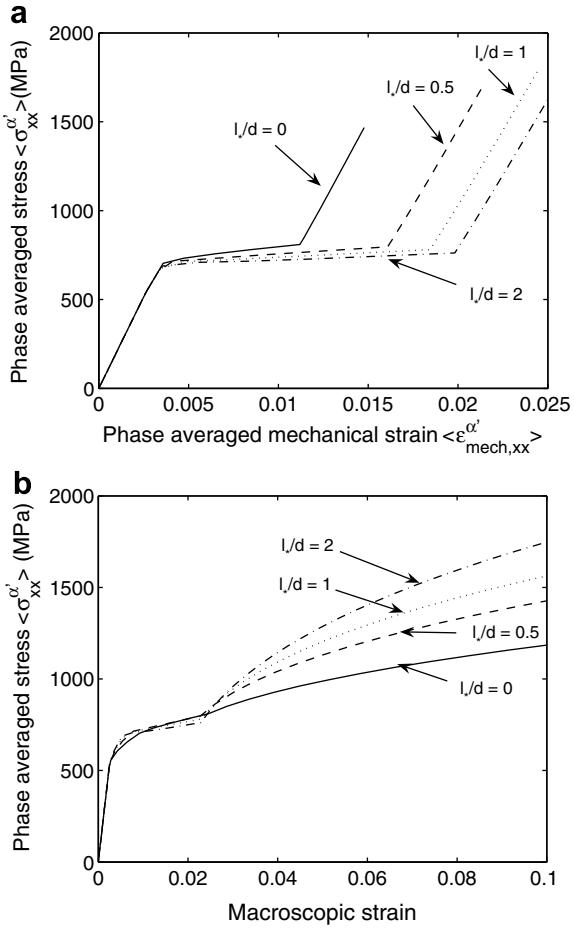

Fig. 10. Variation of the phase averaged stress of the martensite as function of (a) the phase averaged strain and (b) of the averaged strain E for various ratios l_*/d using $f_\gamma = 10\%$, $h/d = 1/3$, $E_{\text{tsf}}^{\text{start}} = 2.25\%$ and for Case No. 2.

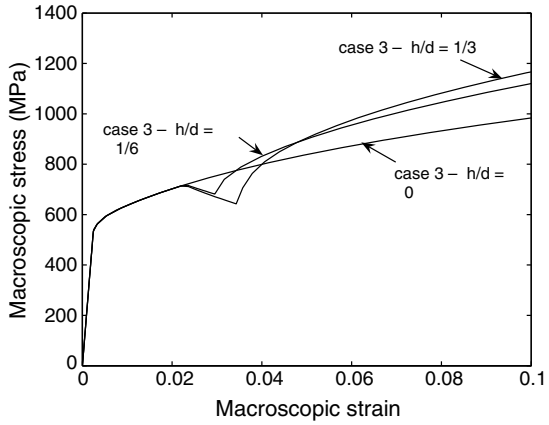

Fig. 11. Influence of the ratio $\frac{h}{d}$ (h, thickness of the martensite plate; d, inclusion size) on the stress strain response along the tensile direction of the representative unit cell with constrained plastic flow at the α'/γ interface and unconstrained plastic flow at the other elasto–plastic boundaries, $f_\gamma = 10\%$, $l_*/d = 1$, $E_{\text{tsf}}^{\text{start}} = 2.25\%$ in Case No. 3.

problem described above. In the case of unconstrained elasto-plastic boundaries, the confinement is lower since the plastically deforming regions (with the same extent) are surrounded by non-constrained boundaries on one side.

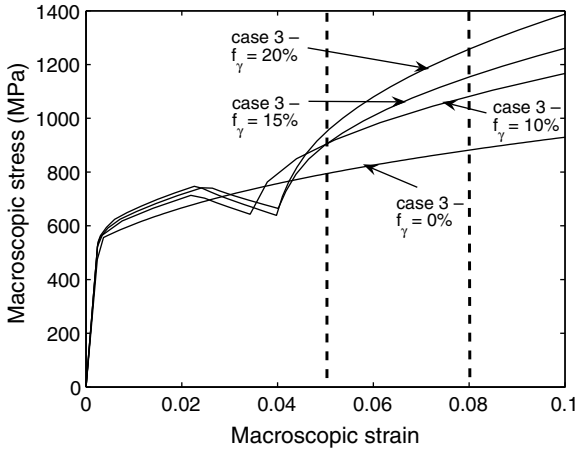

Fig. 12. Influence of f_γ on the stress strain response along the tensile direction of the representative unit cell with constrained plastic flow at the α'/γ interface and unconstrained plastic flow at the other elasto-plastic boundaries, $l_*/d = 1$, $h/d = 1/3$, $E_{tsf}^{start} = 2.25\%$ in Case No. 3.

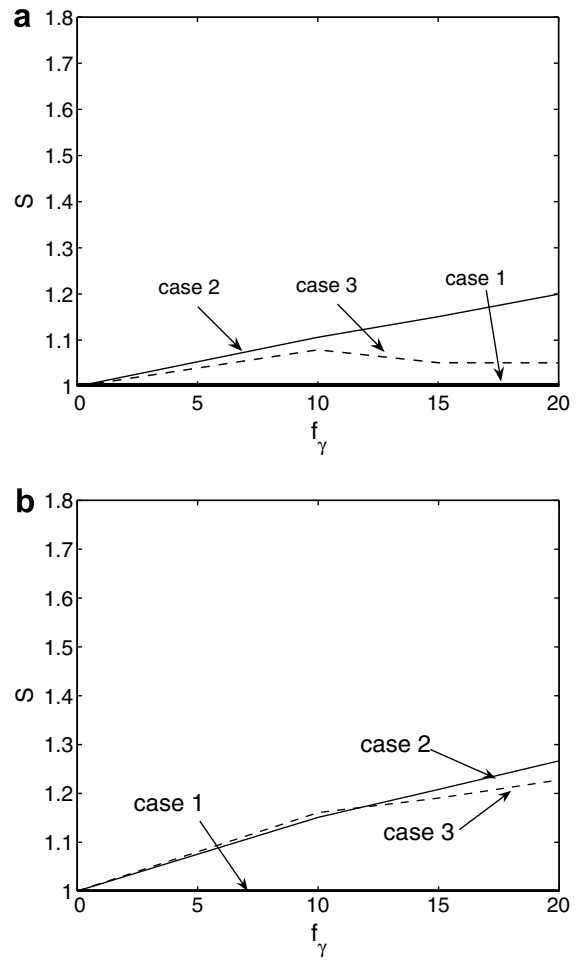

Fig. 13. Variation of the strengthening indicator S as a function of f_γ with constrained plastic flow at the α'/γ interface and unconstrained plastic flow at every other elasto–plastic boundaries, $h/d = 1/3$, $l_*/d = 1$, $E_{tsf}^{start} = 2.25\%$ (a) at $E_{macro} = 5\%$ (b) at $E_{macro} = 8\%$ for Cases No. 1, No. 2 and No. 3.

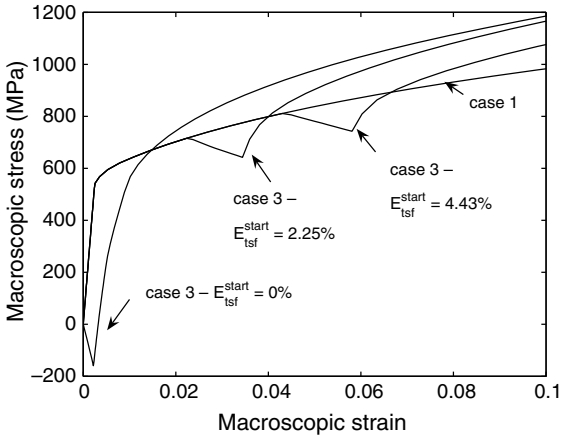

Fig. 14. Influence of E_{tsf}^{start} on the stress strain response along the tensile direction of the representative unit cell with constrained plastic flow at the α'/γ interface and unconstrained plastic flow at the other elasto-plastic boundaries, $l_*/d = 1$, $h/d = 1/3$, $f_\gamma = 10\%$.

The confinement provided by the elastically unloaded regions in the constrained case (equivalent to the shear layer surrounded by two hard substrates) is the main cause of the larger strengthening observed with respect to the unconstrained case due to the presence of strong plastic gradients at these boundaries. These gradients enter the additional non-standard term in the expression of the generalized plastic strain variation $\dot{E}_P$. In Fleck and Hutchinson (2001), the hardness evolution is linked to the total dislocation density which is intended to be represented by the generalized effective plastic strain E_P. As a result, the uniaxial hardening function $h = \frac{d\sigma}{dE_P}$ is evaluated at E_P in order to be consistent with this interpretation.

Fig. 16a and b show contour plots of the variation of the generalized effective plastic strain ΔE_P until the end of the transformation step, from the beginning of the transformation step. The combination of the unloading zones related to the transformation strain and of the local deformation induced by the shear component of the transformation strain leads to the additional plastic flow near the tips of the lenticular plate (top right and bottom left diagonals of the cell) in both constrained (Fig. 16a) and unconstrained (Fig. 16b) cases. In the constrained case however, the additional plastic straining related to the transformation occurs with high confinement between the elastic unloading zones. As a result large generalized plastic strains E_P develop in larger regions of the ferritic phase in the constrained case.

We believe that applying no constraint at the moving elasto-plastic boundary is closer to the physics and that the lower bound on the strengthening effect obtained this way should not be far from the real behavior. Nevertheless, this does not definitely mean that the transformation strain does not affect the strength. Accounting for more than one internal length within the strain gradient plasticity theory could also affect the results significantly. Indeed, the shear component of the transformation strain leads to rotation gradients. In Niordson and Hutchinson (2003b), a few examples show that the use of the three parameters theory gives higher strengthening that the one parameter theory when looking at the shearing of a finite slab. The reasons for the difference in strengthening between the one parameter theory and the multi parameters theory are multiple. First, the measures of the gradients of plastic strain involved in both theories are not the same. As focused in the plane strain shear of a finite slab (Niordson and Hutchinson, 2003b), no gradient effects are taken into account in the vicinity of the free edges when using the one parameter theory framework, as a consequence of the natural boundary condition $\dot{\tau}_i n_i = \dot{\epsilon}_{P,i} n_i = 0$. In the three parameters theory, the gradient of the effective plastic strain is not only taken into account but also the gradient of the complete tensor of plastic strain is involved, resulting in a non-zero contribution at the free edges of the finite slab (Niordson and Hutchinson, 2003b). Second, a significant contribution to the strengthening is brought in by the gradients of the direction of the deviatoric stress m_{ij}. This is illustrated by Niordson (2003a) showing that for a composite involving a short metal fiber in a matrix, the three parameter theory compared to the one parameter theory, leads to lower levels of plastic strain close to the fiber, where gradients of m_{ij} are the largest, and to an enhanced strengthening. In the case of a phase transformation with additional transformation strain, strong gradients in the direction of the stress deviator m_{ij} are expected to play a role. Finally, as explained already in Section 4, a finite strain framework is necessary to extend the calculations to larger strains in order to provide valid results after the transient: the additional transformation strain could contribute more significantly to the strengthening at larger strains.

This discussion also shows that theories including more complete boundary conditions at elasto-plastic boundary, or avoiding the need to prescribe explicitly a constraint on the elasto-plastic boundary are desirable. This point is further discussed in the appendix.

5.2. Size-dependent strengthening from composite effect

The size-dependent strengthening effect coming from the change of properties when the soft inclusion partially transforms into a hard plate is very similar to the size-dependent strengthening associated to hard particles already discussed

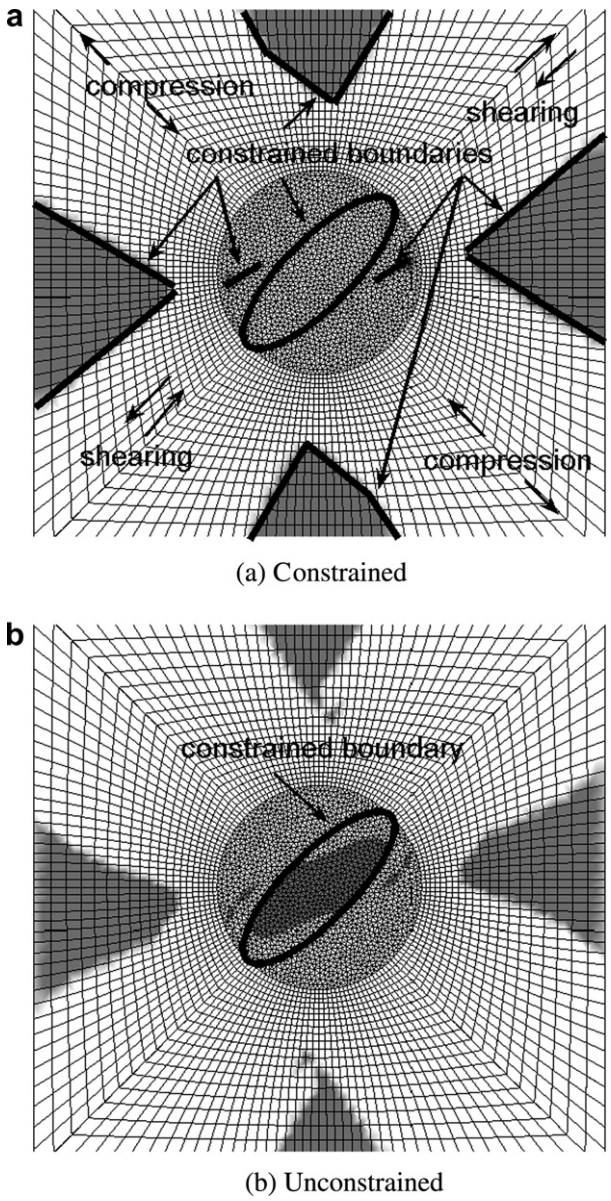

Fig. 15. Contour plot showing the zone undergoing elastic unloading in dark at the end of the transformation step, using $f_\gamma = 10\%$, $h/d = 1/3$, l_*/d=1, $E_{tsf}^{start} = 2.25\%$ in Case No. 3 (a) when the plastic flow is constrained at elasto–plastic boundaries and (b) when the plastic flow is unconstrained at elasto–plastic boundaries. The plastic flow is always fully constrained at the α'/γ interface.

in the literature by many authors (Niordson and Tvergaard, 2001; Niordson, 2003a; Liu and Hu, 2005; Borg et al., 2006). For instance, the results described in Niordson (2003a) involving a hard inclusion within a plastically deforming matrix described by the Fleck–Hutchinson model show a strengthening which increases when the volume fraction of the inclusion increases. With the use of the one parameter theory and a ratio $l_*/r_f = 1$, r_f being the radius of the fiber, and constrained plastic flow at the interface between the fiber and the matrix, a 5% increase in strengthening is obtained with respect to the conventional material without size effect when the volume fraction of the fiber is equal to 13% and when the tensile strain is equal to 8%. These value can be qualitatively compared to our results: Fig. 8b shows that a 7% increase in strengthening is found for $f_\gamma = 10\%$ and $l_*/d = 0.5$, at $E_{macro} = 8\%$. When using the multi-parameter framework, a similar strengthening enhancement with respect to the conventional material is obtained when the three material parameters are set equal to $r_f/2$.

5.3. Size-dependent transformation strain effect

The results of the parametric study show that, even with size-dependent plasticity effects taken into account, the transformation strain seems to play only a limited direct role on the overall strengthening of the material, except if highly con-

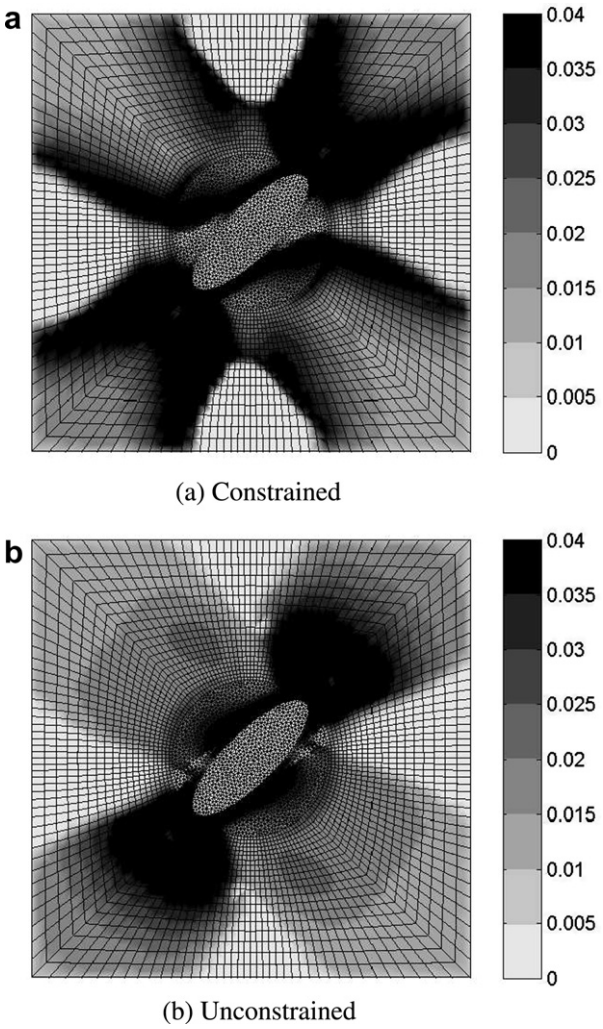

Fig. 16. Repartition, at the end of the transformation step, of the generalized effective plastic strain increment calculated with respect to its value at the beginning of the transformation step, using $f_\gamma = 10\%$, $h/d = 1/3$, l_*/d=1, $E_{tsf}^{start} = 2.25\%$ in Case No. 3 (a) when the plastic flow is constrained at elasto–plastic boundaries and (b) when the plastic flow is unconstrained at elasto–plastic boundaries. The plastic flow is always fully constrained at the α'/γ interface.

strained, and probably not very physical, boundary conditions are imposed on the elasto–plastic boundary. This does not mean that the transformation strain has no effect and should not be taken into account. The transformation strain plays two important roles in the mechanics of transformation induced plasticity. First, Fig. 2 and 9, when compared to Fig. 10, show that the transformation strain leads to large compressive stress into the transformed region, as well as in the surrounding material during and after the transformation. This transient is amplified when taking into account size effects in the case of small transforming regions. The main consequence of this compressive state is to delay the occurrence of damage within the brittle martensite phase. Indeed, the austenite in TRIP-assisted multiphase steels is retained metastable at room temperature owing to high concentration of carbon (typically 1% or more), which is a stabilizing element for the austenite. High level of carbon makes the martensite very brittle. As soon as martensite starts undergoing large tensile stresses, on the order of 1–2 GPa, cracking inside the inclusion or along the interface will occur, initiating the damage process. When these voids or microcracks are nucleated, damage proceeds rapidly with limited amount of void growth and early void coalescence (see Jacques et al., 2001; Lacroix et al., in press). Typical true fracture strains in multiphase TRIP steels are not very high, on the order of 0.5 in a tensile test (see Lacroix et al., in press), leading sometimes to processing problems. Decreasing the austenite grain size would thus not only be beneficial for increasing the strength but also for improving the damage resistance by enlarging the transient during which martensite is not seeing tensile stresses.[1]

[1] As a matter of fact, we anticipate considering the results of Fig. 9, that the typical 1 μm grain size of the austenite in current TRIP-assisted multiphase steels already contributes at improving the damage resistance with respect to a fictitious analogous material with larger grain size.

A second important indirect effect of the transformation strain is on the transformation kinetics by controlling directly the mechanical driving force for the transformation and the elastic and plastic accommodation in the surrounding material, see next subsection. Hence, the transformation strain, by controlling the condition for the transformation, indirectly affects the strengthening too.

5.4. Microstructure optimization

Generating the best TRIP-steels in terms of plastic properties not only depends on the potential extra strengthening of the alloy but also on the kinetics of the transformation and how the transformation spreads along the deformation path. As explained by Lani et al. (2007), if the transformation occurs too rapidly, the extra strain hardening effect resulting from the TRIP mechanism is exhausted too quickly. Conversely, if the transformation is too slow, the extra strain-hardening comes too late and does not contribute to delaying plastic localization. The stability of the retained austenite is primarily dictated by the carbon content, but it is well known that its size (as addressed here), environment and the stress state have also an effect (Lani et al., 2007; Jacques et al., 2007; Jimenez-Melero et al., 2007). Furthermore, better results are always obtained when the transformation spreads for a sufficiently large range of strains to postpone necking. The spreading of the transformation is related to a dispersion in carbon content, sizes and environment among the austenite inclusion.

The predicted enhancement of the TRIP effect when decreasing the size of the retained austenite islands provides a motivation for developing TRIP-assisted multiphase steels with finer microstructures. Nevertheless, one must consider that decreasing the inclusion size tends to delay the transformation. The main reasons are the following (see e.g., Reisner et al., 1998). First, a small inclusion size puts a geometric constraint on the growth of the selected martensite variant. Second, the plastic strain gradients discussed in this paper affect the stress and strain redistribution during the transformation and can lead to an increase of the accommodation terms which act as a dragging force for the transformation. The behavior of the plastic and elastic accommodation terms will be addressed in further studies.

Hence, if a steel is optimized for one inclusion size, one should probably consider decreasing slightly the carbon content if for instance decreasing the inclusion size, in order to keep the same transformation kinetics. A model combining the mechanical behavior of the multiphase material with size effect and a transformation kinetics model, in the vein of the model proposed in Lani et al. (2007) and Delannay et al. (2008), but accounting also for inclusion size (motivated by the present study), is necessary to guide this optimization. The problem becomes even more complex if optimization is also made with respect to the size dependent and transformation kinetics dependent damage behavior of these materials.

6. Conclusions

The effect of transformation induced plasticity (TRIP) on a simplified globular microstructure has been addressed using the Fleck and Hutchinson strain gradient plasticity theory (Fleck and Hutchinson, 2001). A cell made of a ferrite matrix and an austenite inclusion is embedded into an homogenized medium. A portion of the austenite is forced to transformation into a hard martensitic plate with a change of mechanical properties as well as a transformation strain. The important outcomes of this study are:

- The use of strain gradient plasticity theory leads to much larger strengthening related to the TRIP effect than when using a classical plasticity theory. Similar levels of enhancement can be obtained with classical theories by using extra adjustments (e.g., Delannay et al., 2008). Nevertheless, the present framework does not account for multigrain interaction effects with grains transforming at different instants making difficult a direct comparison with experimental data.
- The boundary conditions specified on the plastic flow play a major role regarding the impact of the transformation strain on the strength of the material. Except for the α'/γ interface, the elasto–plastic boundaries have been considered as unconstrained for most of the analyses.
- When the plastic flow is unconstrained, the transformation strain has only a weak effect on the strengthening even with small microstructure features and large volume fractions of austenite. Most of the strengthening comes from the evolving composite effect associated to the presence of a new hard inclusion.

Further works will focus on extensions to finite strain framework and to a three length scale parameter theory.

Acknowledgement

Financial support from Region Wallonne through the convention RW-WINNOMAT program under Grant ACIETRIP 0415961 is gratefully acknowledged.

Appendix.

Among all the theories presented above, the originality of the Fleck and Hutchinson (2001) theory is that the gradients effects are only incorporated in the plastic regime. Consequently, the second field equation (7) is only valid within the plastic domain. A negative consequence thereof is that boundary conditions have to be specified at the elasto-plastic boundaries. Such boundary conditions are still strongly debated in the literature (Niordson and Hutchinson, 2003b) and must be carefully considered. Within an implementation similar to Niordson and Hutchinson (2003b), the effective plastic strain rate $\dot{\epsilon}_P$ or the higher order traction $\dot{\tau}_i n_i$ can be prescribed alternatively at the internal elasto-plastic boundary. As a result these boundary conditions are mutually exclusive in this type of implementation. In Gudmundson (2004), it is suggested to impose $\dot{\epsilon}_P = 0$ at an elasto–plastic boundary to enforce the continuity of the higher order stresses. In Polizzotto (2007) it is shown, using thermodynamical principles, that the proper boundary condition at an elasto-plastic boundary should be that both the effective plastic strain rate and the higher order traction vanish. This is possible only in a C^1 framework implementation or with a penalty-enhanced C^0 interpolation where the plastic strain gradients are interpolated independently (e.g., de Borst and Pamin, 1996).

Finally, non-local theories were recently proposed in which a non-local effective plastic strain $\bar{\epsilon}_P$ entering the yield condition is introduced and evaluated through a partial differential equation (14) incorporating an intrinsic length parameter and the local effective plastic strain ϵ_P (Engelen et al., 2006; Peerlings, 2007):

$$\bar{\epsilon}_P - l_*^2 \bar{\epsilon}_{P,ii} = \epsilon_P. \tag{14}$$

Since this equation is applied on the entire volume of the specimen, no specific boundary conditions need to be specified at the elasto-plastic boundaries. Furthermore, this type of formulation naturally leads to incremental iterative schemes and allows larger time steps within the computations.

In Engelen et al. (2006), the yield condition reads as:

$$\sigma_e \leqslant \sigma_y(\varepsilon_P, \bar{\varepsilon}_P) \tag{15}$$

σ_e being the von Mises effective stress, ε_P the effective plastic strain, $\bar{\varepsilon}_P$ the non-local effective plastic strain. The equation (14) is verified and external boundary conditions on the non-local effective plastic strain are imposed. However, this theory was shown to be well adapted to represent softening size effects, but not for hardening problems. This type of framework was further elaborated in Peerlings (2007) where the yield condition reads as:

$$\sigma_e - \sigma_{y0} - h\varepsilon_P - \bar{h}(\varepsilon_P - \bar{\varepsilon}_P) = 0 \tag{16}$$

with σ_{y0} being the initial yield stress, h the hardening modulus, and $\bar{h}$ an intrinsic parameter. The equation (14) is verified and accompanied with a specific set of boundary conditions:

- the continuity of the effective plastic strain is ensured at the elasto-plastic boundary: $\bar{\varepsilon}_P - l_*^2 \bar{\varepsilon}_{P,ii} = 0$;
- the continuity of the von Mises equivalent stress is ensured at the elasto-plastic boundary;
- boundary conditions on the gradients of non-local effective plastic strain are imposed to respect the eventual symmetries of the problem;
- boundary conditions on the non-local effective plastic strain are imposed at the external boundary of the solid.

Since this framework is only established for linear hardening at present, the Fleck and Hutchinson (2001) gradient was used in the present contribution, despite the debate about boundary conditions on plastic flow at elasto-plastic boundary. It is also strongly motivated by the incremental nature of the Fleck–Hutchinson theory which enables to impose evolving boundary conditions at martensitic/austenitic interface. Since variations of the effective plastic strain and displacements are primarily unknown, the effective plastic strain rate $\dot{\epsilon}_P$ can be easily constrained to vanish at each time step.

References

Abu Al-Rub, R.K., 2007. Prediction of micro and nanoindentation size effect from conical or pyramidal indentation. Mechanics of Materials 39, 787–802.
Aifantis, E.C., 1984. On the microstructural origin of certain inelastic models. Transactions of the ASME. Journal of Engineering Materials and Technology 106 (4), 326–330.
Aifantis, K.E., Ngan, A.H.W., 2007. Modeling dislocation-grain boundary interactions through gradient plasticity and nanoindentation. Materials Science and Engineering: A 459 (1–2), 251–261.
André, N., Coulombier, M., De Longueville, V., Fabrègue, D., Gets, T., Gravier, S., Pardoen, T., Raskin, J.-P., 2007. Microfabrication-based nanomechanical laboratory for testing the ductility of submicron aluminium films. Microelectronic Engineering 84 (11), 2714–2718.
Ball, J.M., James, R.D., 1987. Fine phase mixtures as minimizers of energy. Archive for Rational Mechanics and Analysis 100 (1), 13–52.
Balint, D.S., Deshpande, V.S., Needleman, A., Van der Giessen, E., 2006. Size effects in uniaxial deformation of single and polycrystals: a discrete dislocation plasticity analysis. Modelling and Simulation in Materials Science and Engineering 14, 409–422.
Bhattacharya, K., 1993. Comparison of the geometrically nonlinear and linear theories of martensitic transformation. Continuum Mechanics and Thermodynamics 5 (3), 205–242.
Borg, U., Niordson, C.F., Fleck, N.A., Tvergaard, V., 2006. A viscoplastic strain gradient analysis of materials with voids or inclusions. International Journal of Solids and Structures 43 (16), 4906–4916.

de Borst, R., Mühlhaus, H.B., 1992. Gradient-dependent plasticity: formulation and algorithmic aspects. International Journal for Numerical Methods in Engineering 35, 521–539.
de Borst, R., Pamin, J., 1996. Some novel developments in finite element procedures for gradient-dependent plasticity. International Journal for Numerical Methods in Engineering 39, 2477–2505.
Chen, S.H., Liu, L., Wang, T.C., 2007. Small scale, grain size and substrate effects in nano-indentation experiment of film substrate systems. International Journal of Solids and Structures 44 (13), 4492–4504.
Cherkaoui, M., Berveiller, M., Sabar, H., 1998. Micromechanical modeling of martensitic transformation-induced plasticity (TRIP) in austenitic single crystals. International Journal of Plasticity 14 (7), 597–626.
Dan, W.J., Zhang, W.G., Li, S.H., Lin, Z.Q., 2007a. Finite element simulation on strain-induced martensitic transformation effects in TRIP steel sheet forming. Computational Materials Science 39 (3), 593–599.
Dan, W.J., Zhang, W.G., Li, S.H., Lin, Z.Q., 2007b. A model for strain-induced martensitic transformation of TRIP steel with strain rate. Computational Materials Science 40 (1), 101–107.
Dan, W.J., Li, S.H., Zhang, W.G., Lin, Z.Q., 2008. The effect of strain-induced martensitic transformation on mechanical properties of TRIP steel. Materials and Design 29 (3), 604–612.
Delannay, L., Jacques, P., Pardoen, T., 2008. Modelling of the plastic flow of trip-aided multiphase steel based on an incremental mean-field approach. International Journal of Solids and Structures 45 (6), 1825–1843.
Delincé, M., Jacques, P.J., Pardoen, T., 2006. Separation of size-dependent strengthening contributions in fine-grained Dual Phase steels by nanoindentation. Acta Materialia 54 (12), 3395–3404.
Diani, J.M., Sabar, H., Berveiller, M., 1995. Micromechanical modelling of the transformation induced plasticity (TRIP) phenomenon in steels. International Journal of Engineering Science 33 (13), 1921–1934.
Dong, M., Schmauder, S., 1996. Modeling of metal matrix composites by a self-consistent embedded cell model. Acta Materialia 44 (6), 2465–2478.
Ekh, M., Grymer, M., Runesson, K., Svedberg, T., 2007. Gradient crystal plasticity as part of the computational modelling of polycrystals. International Journal for Numerical Methods in Engineering 72 (2), 197–220.
Engelen, R.A.B., Fleck, N.A., Peerlings, R.H.J., Geers, M.G.D., 2006. An evaluation of higher-order plasticity theories for predicting size effects and localisation. International Journal of Solids and Structures 43 (7-8), 1857–1877.
Evers, L.P., Brekelmans, W.A.M., Geers, M.G.D., 2004. Scale dependent crystal plasticity framework with dislocation density and grain boundary effects. International Journal of Solids and Structures 41 (18–19), 5209–5230.
Fischer, F.D., Reisner, G., 1998. A criterion for the martensitic transformation of a microregion in an elastic plastic material. Acta Materialia 46 (6), 2095–2102.
Fischer, F.D., Reisner, G., Werner, E., Tanaka, K., Cailletaud, G., Antretter, T., 2000. A new view on transformation induced plasticity (TRIP). International Journal of Plasticity 16 (7–8), 723–748.
Fleck, N.A., Muller, G.M., Ashby, M.F., Hutchinson, J.W., 1994. Strain gradient plasticity: theory and experiment. Acta Metallurgica et Materialia 42 (2), 475–487.
Fleck, N.A., Hutchinson, J.W., 1997. Strain gradient plasticity. Advances in Applied Mechanics 33, 295–361.
Fleck, N.A., Hutchinson, J.W., 2001. A reformulation of strain gradient plasticity. Journal of the Mechanics and Physics of Solids 49, 2245–2271.
Fleck, N.A., Ashby, M.F., Hutchinson, J.W., 2003. The role of geometrically necessary dislocations in giving material strengthening. Scripta Materialia 48 (2), 179–183.
Fredriksson, P., Gudmundson, P., 2005. Size-dependent yield strength of thin films. International Journal of Plasticity 21 (9), 1834–1854.
Furnémont, Q., 2003. The Micromechanics of TRIP-Assisted Multiphase Steels. Ph.D. thesis, Université catholique de Louvain, Louvain-la-Neuve.
Ganghoffer, J.F., Simonsson, K., 1998. A micromechanical model of the martensitic transformation. Mechanics of Materials 27 (3), 125–144.
Gudmundson, P., 2004. A unified treatment of strain gradient plasticity. Journal of the Mechanics and Physics of Solids 52 (6), 1379–1406.
Huang, D.W., 2007. Size-dependent response of ultra-thin films with surface effects. International Journal of Solids and Structures 45 (2), 568–579.
Iwamoto, T., Tsuta, T., 2000. Computational simulation of the dependence of the austenitic grain size on the deformation behavior of TRIP steels. International Journal of Plasticity 16 (7–8), 791–804.
Jacques, P.J., Furnémont, Q., Pardoen, T., Delannay, F., 2001. On the role of martensitic transformation on damage and cracking resistance in TRIP-assisted multiphase steels. Acta Materialia 49 (1), 139–152.
Jacques, P.J., 2004. Transformation-induced plasticity for high strength formable steels. Current Opinion in Solid State and Material Science 8 (3–4), 259–265.
Jacques, P.J., Furnémont, Q., Lani, F., Pardoen, T., Delannay, F., 2007. Multiscale mechanics of TRIP-assisted multiphase steels: I. Characterization and mechanical testing. Acta Materialia 55 (11), 3681–3693.
Janssen, P.J.M., de Keijser, T.H., Geers, M.G.D., 2006. An experimental assessment of grain size effects in the uniaxial straining of thin Al sheet with a few grains across the thickness. Materials Science and Engineering: A 419 (1–2), 238–248.
Jimenez-Melero, E., van Dijk, N.H., Zhao, L., Sietsma, J., Offerman, S.E., Wright, J.P., van der Zwaag, S., 2007. Characterization of individual retained austenite grains and their stability in low-alloyed TRIP steels. Acta Materialia 55 (20), 6713–6723.
Keralavarma, S.M., Benzerga, A.A., 2007. A discrete dislocation analysis of strengthening in bilayer thin films. Modelling and Simulation in Materials Science and Engineering 15, 239–254.
Kizler, P., Schmauder, S., 2007. Simulation of the nanoindentation of hard metal carbide layer systems the case of nanostructured ultra-hard carbide layer systems. Computational Materials Science 39 (1), 205–213.
Kouznetsova, V.G., Brekelmans, W.A.M., Baaijens, F.P.T., 2001. An approach to micro-macro modeling of heterogeneous materials. Computational mechanics 27 (1), 37–48. Eindhoven University of Technology.
Lacroix, G., Pardoen, T., Jacques, P.J., 2008. On the fracture toughness of TRIP-assisted multiphase steels. Acta Materialia, doi:10.1016/j.actamat.2008.04.035.
Lani, F., Furnémont, Q., Van Rompaey, T., Delannay, F., Jacques, P.J., Pardoen, T., 2007. Multiscale mechanics of TRIP-assisted multiphase steels: II. Micromechanical modelling. Acta Materialia 55 (11), 3695–3705.
Leblond, J.B., Mottet, G., Devaux, J.C., 1986. A theoretical and numerical approach to the plastic behaviour of steels during phase-transformation – II. Study of classical plasticity for ideal-plastic phases. Journal of the Mechanics and Physics of Solids 34 (4), 411432.
Levitas, V.I., Stein, E., 1997. Simple micromechanical model of thermoelastic martensitic transformations. Mechanics Research Communications 24 (3), 309–318.
Levitas, V.I., Idesman, A.V., Olson, G.B., 1998a. Continuum modeling of strain-induced martensitic transformation at shear-band intersections. Acta Materialia 47 (1), 219–233.
Levitas, V.I., 1998b. Thermomechanical theory of martensitic phase transformations in inelastic materials. International Journal of Solids and Structures 35 (9), 889–940.
Liu, X., Hu, G., 2005. A continuum micromechanical theory of overall plasticity for particulate composites including particle size effect. International Journal of Plasticity 21 (4), 777–799.
Liu, M.X., Ma, F., Huang, P., Zhang, J.M., Xu, K.W., 2007. Scale dependent plastic deformation of nanomultilayers with competitive effects of interphase boundary and grain boundary. Materials Science and Engineering: A. doi:10.1016/j.msea2007.05.040.
Ma, A., Roters, F., Raabe, D., 2006. A dislocation density based constitutive model for crystal plasticity FEM including geometrically necessary dislocations. Acta Materialia 54 (8), 2169–2179.
Marketz, F., Fischer, F.D., 1995. A mesoscale study on the thermodynamic effect of stress on martensitic transformation. Metallurgical and Materials Transactions A 26 (2), 267–278.

Mindlin, R.D., 1964. Micro-Structure in linear elasticity. Archive for Rational Mechanics and Analysis 16 (1), 5178.
Nicola, L., Van der Giessen, E., Needleman, A., 2003. Discrete dislocation analysis of size effects in thin films. Journal of Applied Physics 93, 5920–5928.
Niordson, C.F., Tvergaard, V., 2001. Nonlocal plasticity effects on the tensile properties of a metal matrix composite. European Journal of Mechanics A/Solids 20 (2), 601–613.
Niordson, C.F., 2003a. Strain gradient plasticity effects in whisker-reinforced metals. Journal of the Mechanics and Physics of Solids 51 (10), 1863–1883.
Niordson, C.F., Hutchinson, J.W., 2003b. Non-uniform plastic deformation of micron scale objects. International Journal for Numerical Methods in Engineering 56, 961–975.
Olson, G.B., Cohen, M., 1975. Kinetics of strain-induced martensitic nucleation. Metallurgical and Materials Transactions A 6 (3), 791–795.
Papatriantafillou, I., Agoras, M., Aravas, N., Haidemenopoulos, G., 2006. Constitutive modeling and finite element methods for TRIP steels. Computer Methods in Applied Mechanics and Engineering 195 (37–40), 5094–5114.
Peerlings, R.J.H., 2007. On the role of moving elasticplastic boundaries in strain gradient plasticity. Modelling and Simulation in Materials Science and Engineering 15, S109–S120.
Polizzotto, C., 2007. Strain-gradient elastic–plastic material models and assessment of the higher order boundary conditions. European Journal of Mechanics A/Solids 26 (2), 189–211.
Radmilovic, V., Kilaas, R., Dahmen, U., Shiflet, G.J., 1999. Structure and morphology of S-phase precipitates in aluminum. Acta Materialia 47 (15-16), 3987–3997.
Reisner, G., Werner, E.A., Fischer, F.D., 1998. Micromechanical modeling of martensitic transformation in random microstructures. International Journal of Solids and Structures 35 (17), 2457–2473.
Serri, J., Martiny, M., Ferron, G., 2005. Finite element analysis of the effects of martensitic phase transformation in TRIP steel sheet forming. International Journal of Mechanical Sciences 47 (6), 884–901.
Siska, F., Forest, S., Gumbsch, P., 2007. Simulations of stress strain heterogeneities in copper thin films: Texture and substrate effects. Computational Materials Science 39 (1), 137–141.
Stölken, J.S., Evans, A.G., 1998. A microbend test method for measuring the plasticity length scale. Acta Materialia 46 (14), 5109–5115.
Stringfellow, R.G., Parks, D.M., Olson, G.B., 1992. A constitutive model for transformation plasticity accompanying strain-induced martensitic transformations in metastable austenitic steels. Acta Metallurgia et Materialia 40 (7), 1703–1716.
Tang, H., Schwarz, K.W., Espinosa, H.D., 2007. Dislocation escape-related size effects in single-crystal micropillars under uniaxial compression. Acta Materialia 55 (5), 1607–1616.
Tjahjanto, D.D., Suiker, A.S.J., Turteltaub, S., Rivera Diaz del Castillo, P.E.J., van der Swaag, S., 2007. Micromechanical predictions of TRIP steel behavior as a function of microstructural parameters. Computational Materials Science 41, 107–116.
Tomita, Y., Iwamoto, T., 1995. Constitutive modeling of TRIP steel and its application to the improvement of the mechanical properties. International Journal of Mechanical Sciences 37 (12), 1295–1305.
Toupin, R.A., 1962. Elastic materials with couple-stresses. Archive for Rational Mechanics and Analysis 11 (1), 385–414.
Turteltaub, S., Suiker, A.S.J., 2006. Grain size effects in multiphase steels assisted by transformation-induced plasticity. International Journal of Solids and Structures 43 (24), 7322–7336.
Uchic, M.D., Dimiduk, D.M., Florando, J.N., Nix, W.D., 2004. Sample dimensions influence strength and crystal plasticity. Science 305 (5686), 986–989.
Van Rompaey, T., Lani, F., Jacques, P.J., Blanpain, B., Wollants, P., Pardoen, T., 2006. Three-dimensional computational-cell modeling of the micromechanics of the martensitic transformation in transformation-induced-plasticity-assisted multiphase steels. Metallurgical and Materials Transactions A 37 (1), 99–107.
Weschler, M.S., Lieberman, D.S., Read, T.A., 1953. On the theory of the formation of martensite. Transactions of AIME 197, 1503–1515.
Wei, Z., Yuhua, W., Ning, L., Wenling, X., Shanhua, W., 2007. Directional precipitation of carbides induced by $\gamma/varepsilon$ interfaces in an FeMnSiCrNiC alloy aged after deformation at different temperature. Materials Science and Engineering: A 459 (1–2), 324–329.
Yang, B., Vehoff, H., 2007. Dependence of nanohardness upon indentation size and grain size: a local examination of the interaction between dislocations and grain boundaries. Acta Materialia 55 (3), 849–856.